# Functionalized SWNT/Polymer Nanocomposites for Dramatic Property Improvement

T. RAMANATHAN,[1] H. LIU,[1] L. C. BRINSON[1,2]

[1]Department of Mechanical Engineering, Northwestern University, Evanston, Illinois 60208

[2]Department of Materials Science and Engineering, Northwestern University, Evanston, Illinois 60208

*Received 12 November 2004; revised 11 April 2005; accepted 16 May 2005*
*DOI: 10.1002/polb.20510*
*Published online in Wiley InterScience (www.interscience.wiley.com).*

**ABSTRACT:** In this paper, we present results for polymer nanocomposites of poly(methyl methacrylate) (PMMA) and amide-functionalized SWNTs. The results demonstrate that even at very low loadings, 1 wt % (0.5 vol %), the mechanical and electrical properties are significantly improved. The improvement over PMMA properties exceeds the theoretical bounds for composites with the same volume fraction loading of randomly oriented, straight, individually dispersed nanotubes. The modeling and experimental results thus suggest that the nanotube bundles are well dispersed in the polymer matrix, that the functionalization significantly improves interaction with polymer, and that the interphase formed has improved mechanical properties over that of the matrix material. Loss modulus results indicate a significant difference between functionalized and nonfunctionalized tubes in the composite. Functionalized tubes result in a composite in which relaxation mechanisms are shifted by 30 °C from that of the matrix material, indicating extensive interphase regions and absence of PMMA with bulk properties. Unfunctionalized composites demonstrate a broadening of relaxation modes, but still retain the signature of bulk PMMA properties. These data suggest a morphological difference with a discrete interphase layer in unfunctionalized composites and a fully transformed matrix in the case of functionalization. This difference is consistent with electrical and mechanical property data.  J Polym Sci Part B: Polym Phys 43: 2269–2279, 2005
**Keywords:** functionalized SWNT; PMMA; mechanical properties; electrical properties; dispersion; morphology

## INTRODUCTION

Polymer nanocomposites have received intense attention and research in the past five years, driven by the unique properties of the nanoparticles and potential to create new material systems with superior properties.[1–5] A variety of nanoparticle morphologies have been considered, including spheroidal particles such as silica,[6,7] platelets such as clay[8,9] and graphite,[10–12] and nanotubes including multiwall (MWNT) and single-wall (SWNT) forms.[13–17] Among these, SWNTs have been intensively investigated because of their unique one-dimensional structure with adjustable electric conductivity and robust mechanical properties. Although difficult to measure, based on various experimental approaches as well as molecular dynamic simulations, the tensile strength and modulus of a SWNT are considered to lie in the range of 37–100 GPa and 640 GPa to 1–2 TPa, respectively.[13,15,16,18] These property values are 5–10 times higher than steel, although SWNTs are 1/6th as dense.[19,20] Thus, SWNT-based polymer nanocomposites have the potential to enable development of unique lightweight materials.

*Correspondence to:* L. C. Brinson (E-mail: cbrinson@northwestern.edu)

Journal of Polymer Science: Part B: Polymer Physics, Vol. 43, 2269–2279 (2005)

However, use of nanotube reinforcements in polymer composites has been a challenge because of the difficulties in optimizing the processing conditions to achieve good dispersion and load transfer. Thus, initial published results showed only modest improvement in mechanical properties with MWNT inclusions.[3,21–27] To improve dispersion, several techniques have been attempted, including the use of surfactants,[28] sonication,[25] and other mixing methods.[29] Recent work has demonstrated superior dispersion of MWNTs in polymers by functionalizing the nanotubes to make them compatible with solvents and the matrix material.[26,30–33] The improved dispersion of nanotubes with covalently bonded functional groups has been accompanied by increased mechanical properties of the nanocomposite.

A defining difference between nanoreinforced polymers and polymer composites with traditional micron-sized reinforcements is the extent and influence of the interphase. The extreme surface to volume ratio of the nanoparticles, several orders of magnitude larger than that of micron-sized fillers, and the proximity of size of the nanofiller to the radius of gyration of the host polymers, lead to interphase volume fractions that can easily exceed the volume fraction of the filler phase. With improved dispersion of the nanoparticles in the polymer matrix, the influence of this interphase zone is increased. Recent work[21] has provided visual evidence of the interphase in a MWNT/polycarbonate system, with SEM images illustrating a significant adsorbed polymer layer on nanotubes protruding from fracture surfaces. The existence of this layer indicates a region of significantly altered polymer mobility and behavior, such that during fracture, failure occurred at the interface between this layer and the bulk polycarbonate, as opposed to that at the nanotube–polymer interface. This work also demonstrated an increased size of this region for systems in which the nanotubes had been functionalized before processing the composite. This evidence, combined with mechanical property data, indicates that functionalization leads to an increased interaction zone in polymer nanocomposite systems.

Although the data for MWNT/polymer systems are showing consistently improved mechanical behavior over those for the polymer matrix alone, there are drawbacks to working with MWNTs. In particular, the weak $\pi$–$\pi$ and van der Waals interactions between the shells of MWNTs render the inner tubes less useful mechanically in general loading. Both experimental[34] and modeling[35] work confirm that only the outer shell contributes to the stress–strain response of MWNTs in tensile loading. Although nanotubes in a composite see much more complicated stress states, the added weight of the inner tubes in MWNTs is quite likely not offset by significantly increased property gains. This result leads to consideration of using SWNTs as a filler material. In addition, SWNTs are of particular interest because of their near perfect crystalline structure and incredible mechanical and electrical properties.

In recent literature, some success has been reported in improved mechanical[30,31,36–42] and electrical[25,43–46] properties of SWNT-reinforced polymers as well as enhanced crystallization[47] and orientation of nanotubes.[40] Highlights on mechanical properties of SWNT-reinforced polymer composites are presented in Table 1. Various processing methods have been attempted, including melt mixing (melt blend and melt mixing fiber),[39,40,43] solvent-based method,[31,37,42] *in situ* polymerization,[41] *in situ* functionalization,[30] use of surfactant,[28] and mini-emulsion polymerization.[44] As shown in Table 1, the stiffness increment achieved varies significantly, which is postulated to be heavily dependant on the specific SWNT/polymer systems and different processing methods. Some processing methods, such as *in situ* polymerization, might result in better dispersion of the SWNTs inside the host polymers, leading to improved mechanical properties.

Also among the promising methods is functionalization of SWNTs. Motivated by the success of functionalized MWNTs to improve properties, only few references are available on nanocomposites based on functionalization of SWNTs to date.[30,31] Mitchell et al.[30] reported significant changes in the mechanical behavior of polystyrene (PS) with functionalized SWCNTs using melt rheology. Zhu et al.[31] observed very modest improvements in the solid state (glassy) response using carboxylated SWNTs/epoxy system. In the present work, we used a previously developed method[48] to covalently bond amide functional groups to SWNTs. Nanocomposites are synthesized based on these functionalized SWNTs and poly(methyl methacrylate) (PMMA). Their viscoelastic (glassy to rubbery) mechanical properties are characterized and compared to lit-

**Table 1.** Tabulation of Recent Literature Data on SWNT–Polymer Composites[a]

| Publication | Type of Matrix | Process | CNTs (wt %) | % Increase in *E* |
|---|---|---|---|---|
| Zhu et al.[31] | Epoxy | Solution | "1-unmodified" | 5 |
| | | | 1-COOH | 30 |
| Zhang et al.[36] | PVA-SDS | Film coating | 5 | 60 |
| Putz et al.[41] | PMMA | *In situ* polymerization | <0.1 | 10 |
| Haggenmueller et al.[40] | PMMA | Melt-mixing fiber | 1 | 6 |
| Valentini et al.[39] | IPP/EPDM | Melt blend | 0.25 | 8.7 |
| | | | 0.5 | 17.9 |
| | | | 0.75 | 26 |
| | | | 1 | −13 |
| Lopez-Manchado et al.[38] | CV 60 | Roll mill | 0.1 | 63 |
| Grady et al.[42] | IPP | Solution evaporation | 0.6 | −7.7 |
| | | | 1.8 | 42 |
| Geng et al.[37] | PEO | Solution evaportation | 1 | 3 |
| | | | 4 | 5 |

[a] See also Figure 6.

erature data as well as modeling predictions. The experimental procedures, results, and discussion are outlined in the next sections.

## EXPERIMENTAL

Purified HiPCO SWNTs (Bucky Pearls) used were supplied by Carbon Nanotechnologies, Inc. (CNI, Houston, TX). Poly(methyl methacrylate) (PMMA) with a molecular weight of 350,000 was purchased from Polysciences (Warrington, PA). Solvents *N*-methyl pyrroloidinone (NMP) and methanol were supplied by Fisher Scientific (Honnover Park, IL).

Amide-functionalized SWNTs (a-SWNT) were prepared through carboxylic acid residues, which were introduced by chemical oxidation method, followed by direct coupling of ethylene diamine (the details of this method are described elsewhere[48]). A solution evaporation technique was used to prepare the composites. In this technique, first, the PMMA was dissolved in NMP. In another vial, SWNTs were dispersed in the same solvent (NMP) by bath sonication for 1 h, added to the polymer solution, and again bath-sonicated for 1 h to disperse the SWNT in the polymer. The mixture was subsequently dropped into stirred methanol to remove NMP and filtered through a polytetrafluoroethylene (PTFE) filter paper with a pore size of 10 $\mu$m. In the case of the functionalized tubes, to produce covalent linkages between a-SWNT and PMMA, an additional step was taken after sonication of the a-SWNT and PMMA mixture: the mixture was stirred at 60 °C for 5 h and then cooled to room temperature before continuing with the antisolvent and filtration. The proposed reaction scheme is shown in Figure 1. For both types of nanocomposites, the products were dried at 80 °C under vacuum for 10 h and then broken into small pieces. These small pieces were placed on a steel mold, covered with a steel plate, and pressed in a hydraulic hot-press at a pressure of 2000 Pa and a temperature of 210 °C for 10 min; they were then cooled down to room temperature. The thickness of the

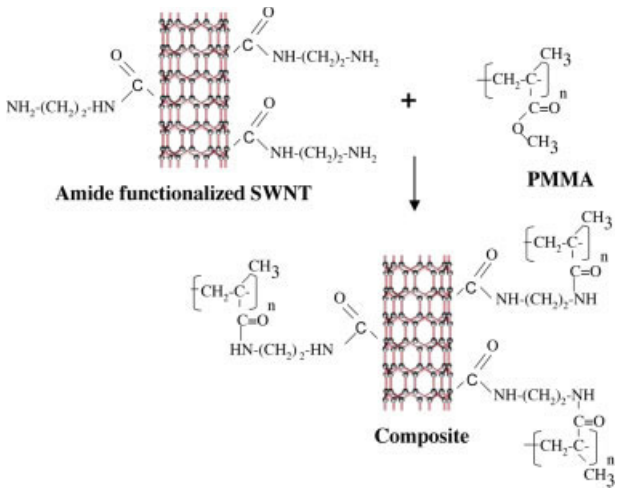


**Figure 1.** Proposed reaction scheme of amide-functionalized SWNT and PMMA composite. [Color figure can be viewed in the online issue, which is available at www.interscience.wiley.com.]

resulting composite film was 0.12 mm. The composites used in this study are 1 wt % (0.5 vol %) of (i) unmodified SWNT and (ii) a-SWNT. Control samples of pure PMMA were prepared following the same procedures.

To verify that the PMMA is covalently bonded to the functionalized nanotubes, Fourier transform infrared (FTIR) spectra of the nanocomposite powder samples were examined before hot pressing. For these tests, the powder samples were washed multiple times with NMP and centrifuged to remove unbound PMMA. After subsequent washing in methanol and dried, IR spectra was recorded using a FTIR Bio-Rad F60 (Bio-Rad Laboratories, Inc., Hercules, CA).

To characterize the thermomechanical properties, thermogravimetric analysis (TGA) of all samples was performed on a TA instrument model TGA-DTA 2960. A small sample (~7 mg) was heated under nitrogen from room temperature to 800 °C at a heating rate of 10 °C/min. Mechanical properties of the samples with a dimension of 12 mm × 6 mm × 0.12 mm were tested by dynamic mechanical analysis (DMA) on a TA Instruments (New Castle, DE) DMA 2980 machine with tension clamp. Temperature sweeps were used to measure the glass transition temperature ($T_g$), and storage and loss modulus curves were recorded. The samples were subjected to sinusoidal strain at a frequency of 1 Hz, and the temperature was ramped up from room temperature to 170 °C at 3 °C/min.

For electrical characterization, AC impedance at room temperature was measured using a Solartron 1290 (Hampshire, UK) impedance analyzer with 1296 dielectric interface. The sample was sandwiched between two rectangular copper electrodes (with a dimension of 21 mm × 6 mm) held tight to the specimen by two flat polycarbonate plates. Electrically conductive paste (colloidal graphite supplied by TED PELLA, Inc., Redding, CA) was applied between the copper electrode and the sample to eliminate the point contacts due to the surface roughness of the polymer surface. LEO 1525 Gemini SEM is (Omicron Nanotechnology, Taunusstein, Germany) used to study the dispersion of SWNT in the polymer.

## RESULTS AND DISCUSSION

IR spectra are shown in Figure 2 for (a) a-SWNT, (b) PMMA, and (c) the a-SWNT/PMMA composite

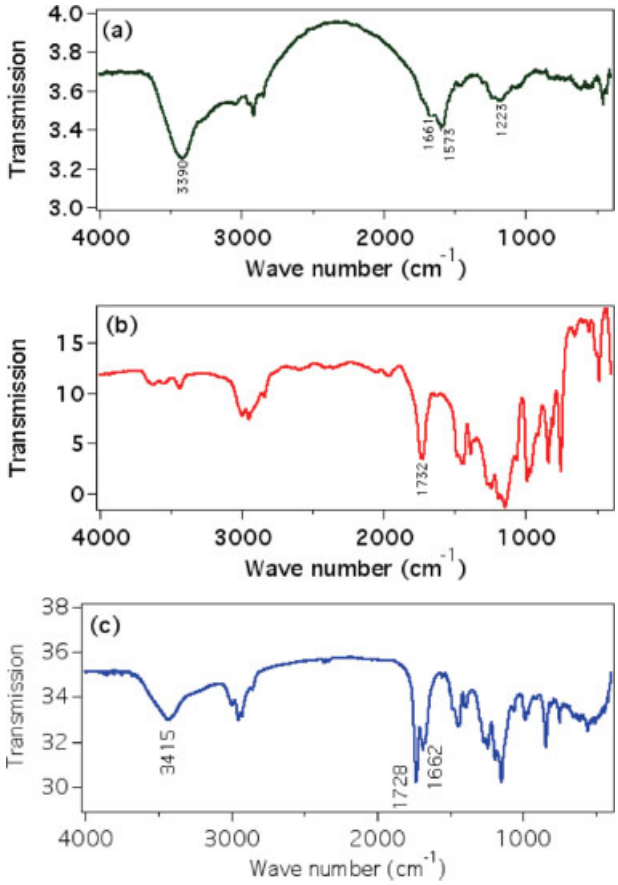


**Figure 2.** FTIR spectrum of (a) a-SWNT only, (b) PMMA only, and (c) a-SWNT–PMMA composites. [Color figure can be viewed in the online issue, which is available at www.interscience.wiley.com.]

after multiple washing with NMP to remove unbonded PMMA. As shown in Figure 2a, the amide carbonyl (—NH—C=O) stretch in functionalized SWNTs is present at ~1661 $cm^{-1}$. The peak at 3390 $cm^{-1}$ corresponds to the $NH_2$ stretch and peaks at 1573 and 1223 $cm^{-1}$ correspond to the N—H in-plane and C—N bond stretching, respectively, in amide-functionalized SWNT.[48] In Figure 2b, the band at ~1732 $cm^{-1}$ is attributed to the ester bond (O—C=O) in PMMA and the $CH_2$ stretch appears at around 2900 $cm^{-1}$. As shown in Figure 1, the ester groups (—O—C=O) in PMMA react with the free amine ($NH_2$) groups in the functionalized SWNTs. As a result, some ester bonds in PMMA have been converted into amide bonds (—NH—C=O). The peak at 1662 $cm^{-1}$ represents the amide bonds from both the functionalized SWNT and the bonded sites of the PMMA molecules. The peak at 1728 $cm^{-1}$ indicates the existence of the ester groups in the washed composite, providing further evidence of

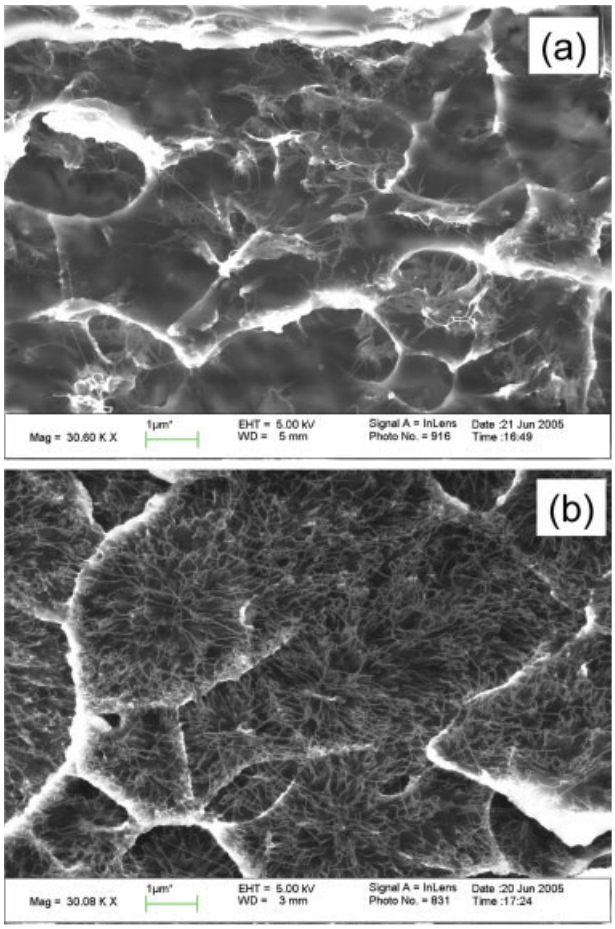


**Figure 3.** SEM images of fracture surface of nanocomposites showing the dispersion of SWNTs in PMMA. (a) clusters of tubes in 1 wt % SWNT/PMMA and (b) improved dispersion in 1 wt % a-SWNT/PMMA.

PMMA bonded to the a-SWNTs: after multiple washing with NMP, all unbonded PMMAs are removed, and thus these ester groups belong to PMMA long chain molecules that have been partially bonded to the a-SWNTs. In addition, the peak at 3415 $cm^{-1}$ corresponds to $NH_2$ stretch mode, which is attributed to the unreacted (with PMMA) $NH_2$ groups on the functionalized SWNTs present in the composites. Taken together, all this evidence confirms the formation of linkage between the free amines ($NH_2$) in the amide-functionalized SWNTs and PMMA, which suggests that free amine ($NH_2$) in functionalized SWNTs can provide an *in situ* chemical integration of the nanotubes and the PMMA molecules as indicated in Figure 1. The types of interactions between PMMA and the SWNTs demonstrated here could improve the interfacial bonding between nanotubes and the polymer, and locally change the nature of the polymer relaxation modes.

An indication of the nanotube dispersion achieved is illustrated in Figure 3. Close examination of fracture surface of 1 wt % SWNT/PMMA composites (fractured using Minimat (TA Instruments, New Castle, DE) at the loading rate of 0.2 mm/min at room temperature) using SEM reveals clusters of SWNTs with a few protruding bundles, shown in Figure 3a. Meanwhile, as can be seen in the SEM image of fracture surface of 1 wt % a-SWNT/PMMA composites shown in Figure 3b, functionalization significantly improves the dispersion, and the dispersed a-SWNTs thus form a good reinforcement network in the polymer. Similar improvement in dispersion of SWNTs in epoxy matrix by functionalization was reported by Zhu et al.[31] but in a less significant fashion. The better dispersion of the a-SWNTs corresponds to an increased number of individual reinforcements in the composite and thus should lead to an increased volume fraction of altered polymer near the nanotubes as well as improved load transfer to a larger volume fraction of nanotubes. Thus, we expect increased thermomechanical properties for the a-SWNT/PMMA composites than for the unfunctionalized SWNT/PMMA composites.

Thermal degradation of pure PMMA and composites are shown in Figure 4. The TGA traces show a significant shift of the weight loss toward higher temperature for both unmodified and amide-functionalized SWNT/PMMA composites, with stabilization 50 °C higher than that

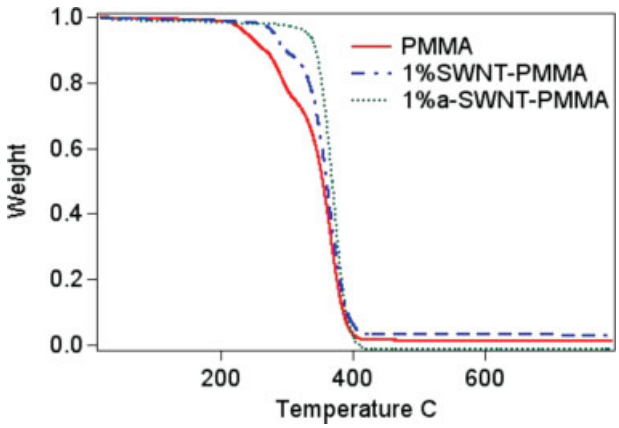


**Figure 4.** Thermogravimetric analysis of PMMA and its composites. Around 7 mg initial weight was used for this study, and normalized values are given for a comparison. [Color figure can be viewed in the online issue, which is available at www.interscience.wiley.com.]

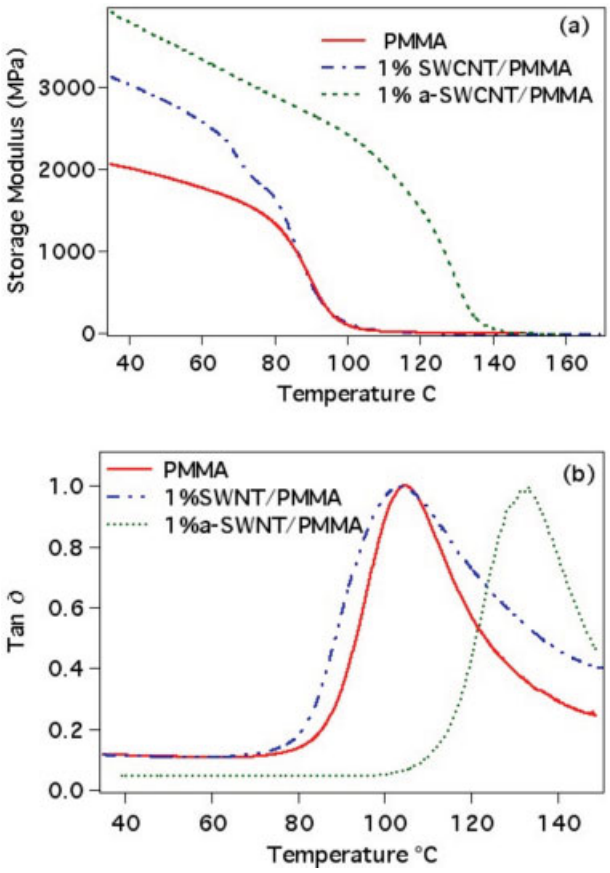


**Figure 5.** DMA results of the average of five test samples. (a) storage modulus and (b) tan $\delta$ with temperature sweep. [Color figure can be viewed in the online issue, which is available at www.interscience.wiley.com.]

for the neat polymer. The improved thermal stability of SWNT/PMMA composites is quite likely associated with the interaction between polymer and SWNTs, as will be explained later in this section.

DMA results are shown in Figure 5 for temperature sweeps of pure PMMA in comparison with those of the nanocomposites. It can be seen that magnitudes of the storage modulus and location of the loss peak change significantly for the nanocomposites. $T_g$s can also be derived from DMA data, and in this work were taken to be at the tan $\delta$ peak. These results (the average of five test samples) are presented in Table 2, along with the magnitudes of the storage modulus at room temperature. The higher deviation in the test results for unmodified and functionalized SWNT is probably due to the less uniform distribution of SWNTs in the samples.

By molecular dynamics simulations, Wei et al.[49] calculated the density variations as a function of temperature for polymer and polymer surrounding a SWNT. The discontinuity in the $\rho$–$T$ plot shows that the $T_g$ increases for the polymer chains in proximity to a nanotube, indicating reduced dynamics of the polymer chains. By analogy to recent work on copolymers, the local heterogeneity in nanocomposites with well-dispersed nanotubes may lead to broadening of the $T_g$.[50] In the present study, for the unmodified SWNT composite, interaction between the SWNT and the PMMA molecules may thus create an interfacial zone of polymer with reduced mobility. This reduced mobility material, in turn, causes an increase in the thermal properties of the composite. The functionalized composite system should have a stronger interfacial bonding between PMMA and SWNTs via their covalent linkages when compared with that in unmodified SWNT/PMMA composites. This strong interaction will further hamper the dynamics of the polymer chains, hindering segmental motion, and thus lead to the higher $T_g$ observed for a-SWNT/PMMA composite than for unmodified SWNT/PMMA composite.

The storage modulus curves (Fig. 5a) show an increase in the glassy modulus by 48% for unmodified SWNT and 86% for a-SWNT composite when compared with that for PMMA. Here, we focus on the change in glassy modulus, as the rubbery response is more easily influenced by the nanotubes, and most potential applications of nanotubes in composites rely on enhanced glassy behavior. These results are consistent with those of Zhu et al.[31] in illustrating the benefit of nanotube functionalization to improve mechanical properties. The further improvement of the modulus is due to a combination of stronger interaction between the functionalized tubes and PMMA, increased extent of the interphase (see tan $\delta$ results given later), and better dispersion of the nanotubes (see Fig. 3b).

The results of the present study are remarkable when compared with simple micromechanical calculations of effective properties. For effec-

**Table 2.** Experimental Results of PMMA and Its Composites

| Sample | $T_g$ by DMA (°C) | Storage Modulus (GPa) at RT |
|---|---|---|
| PMMA | 105 ± 2 | 2.1 ± 0.1 |
| SWNT–PMMA | 105 ± 3 | 3.1 ± 0.3 |
| a-SWNT–PMMA | 138 ± 2 | 3.9 ± 0.6 |

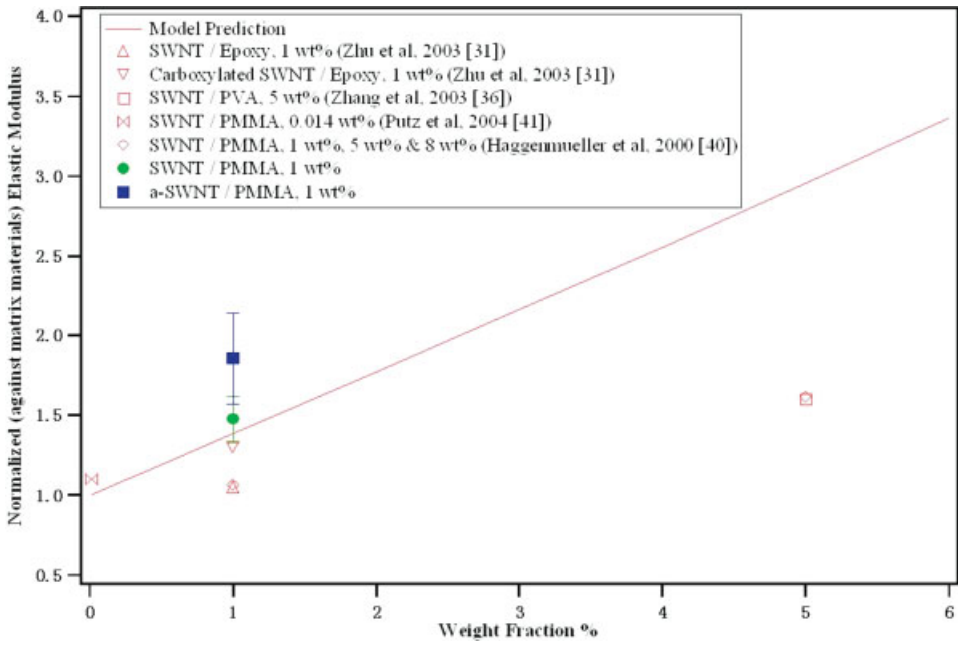


**Figure 6.** Theoretical prediction by Mori–Tanaka model versus experimental results for the modulus values of nanocomposites. The solid line shows the theoretical upper bound of normalized modulus values. The data for the composites presented here exceed this upper bound, indicating significant interphase region with polymer of altered mobility and increased effective stiffness. [Color figure can be viewed in the online issue, which is available at www.interscience.wiley.com.]

tive moduli predictions, a Mori–Tanaka method[51] was employed. The nanotubes were modeled as straight tubular inclusions ideally dispersed in the polymer, with a 3D random orientation distribution. Both the nanotubes and the polymer matrix were treated as isotropic, with ideal nanotube modulus properties of 1 TPa. The interfacial bonding between the inclusions and the matrix was assumed to be perfect. Such a prediction provides an upper bound on two-phase nanocomposites, as imperfections of the physical system that are not considered (curved tubes,[52,53] poor dispersion, and poor interfacial bonding) would serve to decrease modulus predictions. The predicted effective properties at different weight fractions are normalized against the property of the matrix and plotted in Figure 6. As can be seen in the figure, the model predicts that after the incorporation of 1 wt % SWNTs, the modulus increases by 39%. The measured properties for the SWNT/PMMA and a-SWNT/PMMA composites significantly exceed this value. In conjunction with previous results, this data suggests the existence of a significant interphase region in which the polymer properties have been altered by the interaction with the nanoscale inclusions. Another possible contributing factor to this extraordinary behavior could be partial alignment of the nanotubes during the hot pressing. Functionalized SWNTs may be more susceptible to the influence of the melt flow during hot pressing because of their functional groups, a scenario similar to what had been previously observed in macrosized fiber composite processing.[54] Although difficult, further experiments to characterize the orientation distribution of SWNTs in the composites are warranted.

As seen in Figure 6 and Table 1, the increase in storage modulus for the nanocomposite in this work is also significant when compared with previously published data on SWNT-reinforced glassy polymers. Increases in modulus have been predominately modest and lie below simple micromechanical predictions of possible properties, with the exception of the present study and one other. In the work of Putz et al.[41] SWNT/PMMA nanocomposites synthesized via *in situ* polymerization show a 10% increase in storage modulus at room temperature for less than 0.1 wt % SWNT. Thus, this result also lies above the predicted upper bound and could be due to effective crosslinking of the tubes in the polymer network due to the *in situ* polymeriza-

tion process. Similar conclusions were drawn in the works regarding existence of altered polymer near the nanotubes.

Presuming the existence of this interphase region, that the modulus increase for most of the nanocomposites reviewed is considerably lower than the prediction can be attributed to (1) insufficient dispersion of nanotubes, (2) weaker interphase (compared with bulk matrix material), and (3) poor interfacial contact. Although no direct evidence is available to support or disprove the latter two hypotheses, poor dispersion of nanotubes has been shown to correlate with lower modulus[31] and is believed to play a dominant role in controlling the effective properties of the composites. Agglomeration of the nanotubes results in a decrease in the effective surface area to weight (or volume) ratio, which, in turn, results in a decreased amount of altered polymer. Agglomeration also decreases the efficiency of the load transfer to the nanotubes, as interior tubes are not in contact with the polymer. Both of these factors can impede the increase of the effective properties of the composites. The importance of dispersion is reflected in the work of Haggenmueller et al.[40] Polarized Raman spectra on their melt-spun SWNT/PMMA fiber composites suggest that the nanotubes are well aligned, which is expected to lead to a high modulus increase in the fiber axis direction. Yet, the observed increase in modulus is only ~6% at 1 wt % SWNT, far below the predictions for 3D random orientation distribution of nanotubes, and much farther below the prediction for aligned nanotube composites. It is hypothesized that although melt mixing promotes dispersion, the nanotubes in their film and melt-spun fiber composites remained in bundles. The clustering of tubes leads to the decrease of the interphase and insufficient load transfer to inner tubes and thus offsets the property gain from the alignment.

Tan $\delta$ and loss modulus results indicate a significant difference between functionalized and nonfunctionalized nanotubes in the composite. Figure 5b shows the normalized tan $\delta$ curves of the samples. The tan $\delta$ peak for the a-SWNT/PMMA composite is shifted to a higher temperature by 30 °C, corresponding to the large increase in $T_g$. The absence of any loss peak at the PMMA value of 105 °C indicates that in the a-SWNT/PMMA composite the modified polymer with reduced dynamics extends throughout the sample, spanning the region between nanotubes, and that little PMMA with bulk properties remains. For the unmodified SWNT/PMMA composite, the tan $\delta$ peak broadens, but the peak is at the 105 °C value of bulk PMMA. This result is attributed to the existence of a significant amount of unmodified PMMA, due to the clustering of nanotubes, as observed in the SEM images (Fig. 3a). These data suggest a morphological difference with a discrete interphase zone in unfunctionalized SWNT/PMMA composites and a fully transformed matrix in functionalized SWNT/PMMA composites, as illustrated schematically in Figure 7. This difference is also consistent with data for both electrical and mechanical properties.

Modification of the electrical properties of polymers by introduction of inorganic reinforcements such as carbon black and iron powders has long been pursued by researchers.[55–57] Owing to their high aspect ratio, well-dispersed carbon nanotubes can reach the conductivity threshold at smaller loading levels and can create networks that facilitate electron transport. Real impedance, which represents the resistance of the material, is shown in Figure 8, in a frequency sweep between 0.01 and $10^6$ Hz. Although the percolation threshold has not been reached at this loading, the impedance spectrum shows that the low frequency resistance of the film decreases with incorporation of SWNTs in PMMA.

These results agree well with the results of Barraza et al.[44] on SWNT-filled PS composites, in which a percolation threshold between 4 and 8.5 wt % was reported and lower conductivities were attributed to adsorbed polymer on the nanotube bundles. Their results also illustrate an effect of film thickness on impedance beyond the usual calculation for resistivity and suggest that the formation of a well-connected 3D nanotube network is inhibited in the thicker samples. Valentini et al.[58] showed that an amine-functionalized SWNT/epoxy composite increases conductivity, and they discussed mechanisms for charge migration during and after the curing process that lead to the enhanced conductivity. The results of the present study demonstrate that amide-functionalized SWNTs improve the conductivity of the composites beyond SWNTs alone. Work in the sensors area has reported that functionalization of nanotubes can either decrease or increase their electrical response.[59,60] The present result can be attributed to (1) improved dispersion in the a-SWNT

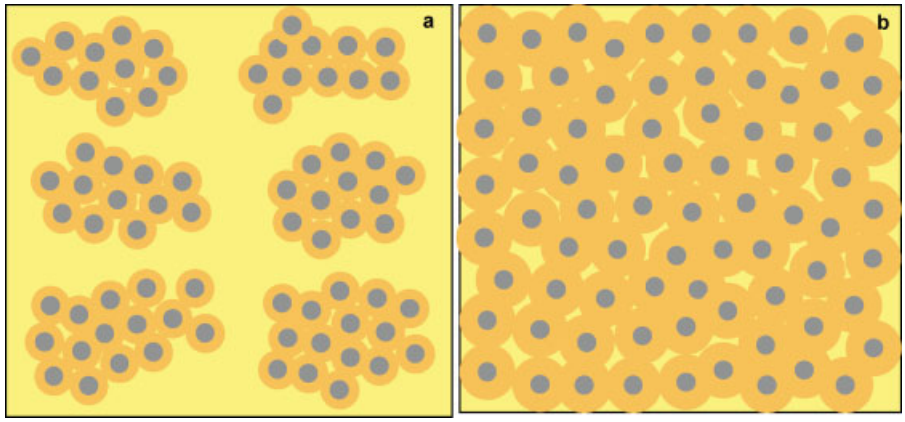


**Figure 7.** Schematic of local morphology and extent of interphase zone in the nanocomposites: (a) unfunctionalized system has local clustering of nanotubes, resulting in tube-rich/tube-poor regions, and a confined influence of polymer interphase and (b) functionalized system has improved nanotube dispersion and larger interphase/zone of influence, resulting in a fully transformed matrix material. [Color figure can be viewed in the online issue, which is available at www.interscience.wiley.com.]

composite, leading to improved connectivity of a nanotube network and (2) interaction between amide groups and SWNTs that may increase conductivity (nanotubes are good electron acceptors because of their structural similarity to fullerenes, whereas an amide is a fairly good electron donor). At this point, the understanding of the mechanism of electron transfer between the functionalized species and nanotubes and its influence on the conductivity of polymer composite is an interesting phenomenon, and further investigation is warranted.

## CONCLUSIONS

In this paper, we described the use of SWNTs to create low volume fraction polymer composites with dramatically improved mechanical, thermal, and electrical properties when compared with those of the neat polymer. Composites were created with unmodified and amide-functionalized the SWNTs. The formation of amide groups on the surface of SWNTs provides free amine groups to interact with PMMA, and IR spectra indicated covalent bonding between a-SWNT and PMMA. For both SWNT/PMMA and a-SWNT/PMMA composites, thermal, mechanical, and electrical data showed significantly improved properties when compared with those of the neat polymer.

The experimental results also demonstrated that the a-SWNT/PMMA composite properties are consistently improved when compared with those of the SWNT/PMMA composite. The increase in thermal degradation temperature, $T_g$, storage modulus, and electrical conductivity confirms better interaction between the functionalized SWNTs and the polymer. The functionalized composite demonstrated a shift in relaxation characteristics by 30 °C relative to the matrix material with no tan $\delta$ peak at the matrix temperature. This result suggests formation of an extensive interphase region of reduced molecular mobility in the vicinity of the nanotubes that penetrates throughout the composite, leaving very little bulk polymer. In contrast, the composite with unmodified nanotubes retained

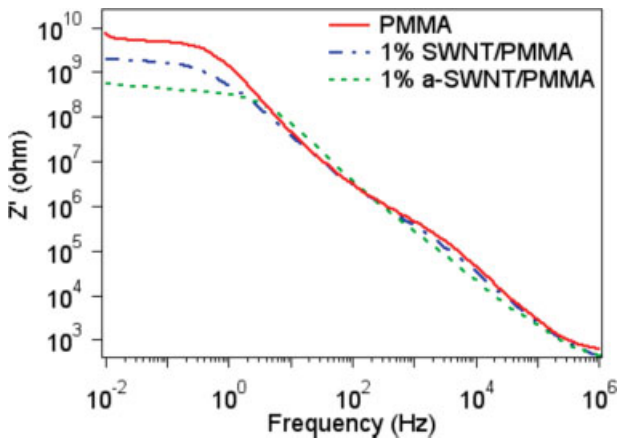


**Figure 8.** AC electrical impedance of nanocomposite, with frequency sweep at RT. [Color figure can be viewed in the online issue, which is available at www.interscience.wiley.com.]

the dominant relaxation characteristics of the bulk PMMA with a broadening of the loss peak, indicating existence of discrete interphase regions near the nanotubes.

The mechanical property data were compared with modeling predictions based on ideal dispersions of randomly oriented straight SWNTs in PMMA. The modulus properties for both composites significantly exceed the predicted upper bound. These results reinforce the existence of an extensive polymer interphase in both composites with altered properties. These results further demonstrate that the altered polymer near the nanotubes has increased modulus, consistent with the loss modulus data indicating decreased mobility of the polymer in the interphase region. The consistent improvement in the properties of the a-SWNT composite when compared with those of the SWNT composite can be attributed to the increased extent of the interphase with altered properties and finer dispersion of nanotubes due to the functionalization.

The results here indicate promising potential for polymer nanocomposites with enhanced thermal, mechanical, and electrical properties. The demonstrated importance of the interphase region underscores the need for more detailed modeling and characterization to understand the changes in local polymer dynamics near nanoparticles and the percolation of these effects in distributed systems. The success of the functionalization to provide consistently improved properties in this work indicates the possibility to create designer nanocomposites with controlled interface chemistry and interphase zones and thus controlled load transfer and properties.

The authors thank Dr. Frank T. Fisher for his valuable advice throughout the duration of the project. We gratefully acknowledge the grant support from the NASA University Research Engineering and Technology Institute on Bio-Inspired Materials (BIMat), under award No. NCC-1-02037.

## REFERENCES AND NOTES

1. Ajayan, P. M.; Schadler, L. S.; Giannaris, C.; Rubio, A. Adv Mater 2000, 12, 750–753.
2. Bower, C.; Rosen, R.; Jin, L.; Han, J.; Zhou, O. Appl Phys Lett 1999, 74, 3317–3319.
3. Jin, Z. X.; Paramoda, K. P.; Xu, G. Q.; Goh, S. H. Chem Phys Lett 2001, 337, 43–47.
4. Lourie, O.; Wagner, H. D. Compos Sci Technol 1999, 59, 975–977.
5. Rao, A. M.; Richter, E.; Bandow, S.; Chase, B.; Eklund, P. C.; Williams, K. A.; Fang, S.; Subbaswamy, K. R.; Menon, M.; Thess, A.; Smalley, R. E.; Dresselhaus, G.; Dresselhaus, M. S. Science 1997, 275, 187–191.
6. Inoue, S. I.; Morita, K.; Asai, K.; Okamoto, H. J Appl Polym Sci 2004, 92, 2211–2219.
7. Liu, Q.; Ding, J.; Chambers, D. E.; Debnath, S.; Wunder, S. L.; Baran, G. R. J Biomed Mater Res 2001, 57, 384–393.
8. Lu, J. K.; Ke, Y. C.; Qi, Z. N.; Yi, X. S. J Polym Sci Part B: Polym Phys 2001, 39, 115–120.
9. Zera, A. S.; Lesser, A. J. J Polym Sci Part B: Polym Phys 2001, 39, 1137–1146.
10. Xiao, M.; Sun, L.; Liu, J.; Li, Y.; Gond, K. Polymer 2002, 43, 2245–2248.
11. Brazhkin, V. V.; Lyapin, A. G.; Popova, S. V.; Klyue, Y. A.; Naletov, A. M. J Appl Phys 1998, 84, 219–226.
12. Chen, G.; Weng, W.; Wu, D.; Wu, C. Eur Polym J 2003, 39, 2329–2335.
13. Falvo, M. R.; Clary, C. J.; Taylor, R. M.; Chi, V.; Brooks, F. P.; Washburn, S.; Superfine, R. Nature (London) 1997, 389, 582–584.
14. Ruoff, R. S.; Lorents, D. C. Carbon 1995, 33, 925–930.
15. Treacy, M. M. J.; Ebbesen, T. W.; Gibson, J. M. Nature (London) 1996, 381, 678–680.
16. Wong, E. W.; Sheehan, P. E.; Lieber, C. M. Science 1997, 277, 1971–1975.
17. Yu, M. F.; Lourie, O.; Dyer, M. J.; Moloni, K.; Kelly, T. F.; Ruoff, R. S. Science 2000, 287, 637–640.
18. Salvetat, J. P.; Andrew, G.; Briggs, D.; Bonard, J. M.; Bacsa, R. R.; Kulik, A. J. Phys Rev Lett 1999, 82, 944–947.
19. Andrews, R.; Jacques, D.; Rao, A. M.; Rantell, T.; Derbyshire, F.; Chen, Y.; Chen, J.; Haddon, R. C. Appl Phys Lett 1999, 75, 1329–1331.
20. Berber, S.; Know, Y. K.; Tomanek, D. Phys Rev Lett 2000, 84, 4613–4616.
21. Eitan, A.; Fisher, F. T.; Andrews, R.; Brinson, L. C.; Schadler, L. S. Compos Sci Technol, to appear in 2005.
22. Thostenson, E. T.; Ren, Z.; Chou, T. W. Compos Sci Technol 2001, 61, 1899–1912.
23. Thostenson, E. T.; Chou, T. W. J Phys D: Appl Phys 2002, 35, 77–80.
24. Schadler, L. S.; Giannaris, S. C.; Ajayan, P. M. Appl Phys Lett 1998, 73, 3842–3844.
25. Sandler, J.; Shaffer, M. S. P.; Prasse, T.; Bauhofer, W.; Schulte, K.; Windle, A. H. Polymer 1999, 40, 5967–5971.
26. Shaffer, M. S. P.; Koziol, K. Chem Commun 2002, 18, 2074–2075.
27. Shaffer, M. S. P.; Windle, A. H. Adv Mater 1999, 11, 937–941.
28. Gong, X.; Liu, J.; Baskaran, S.; Voise, R. D.; Young, J. S. Chem Mater 2000, 12, 1049–1052.

29. Velasco-Santos, C.; Martinez-Heranndez, A. L.; Fisher, F. T.; Ruoff, R. S.; Castano, V. M. J Phys D: Appl Phys 2003, 36, 1423–1428.
30. Mitchell, C. A.; Bahr, J. L.; Arepalli, S.; Tour, J. M.; Krishnamoorti, R. Macromolecules 2002, 35, 8825–8830.
31. Zhu, J.; Kim, J.; Peng, H.; Margrave, J. L.; Khabashesku, V. N.; Barrera, E. V. Nano Lett 2003, 3, 1107–1113.
32. Eitan, A.; Jiang, K.; Dukes, D.; Andrews, R.; Schadler, L. S. Chem Mater 2003, 15, 3198–3201.
33. Halicioglu, T.; Jaffe, R. L. Nano Lett 2002, 2, 573–575.
34. Ding, W.; Eitan, A.; Chen, X.; Dikin, D. A.; Fisher, F. T.; Andrews, R.; Brinson, L. C.; Schadler, L. S.; Ruoff, R. S. Nano Lett 2003, 3, 1593–1597.
35. Belytschko, T.; Xiao, S. P.; Schatz, G. C.; Ruoff, R. Phys Rev B 2002, 65, 235430.
36. Zhang, X.; Liu, T.; Sreekumar, T. V.; Kumar, S.; Moore, V. C.; Hauge, R. H.; Smalley, R. E. Nano Lett 2003, 3, 1285–1288.
37. Geng, H.; Rosen, R.; Zheng, B.; Shimoda, H.; Fleming, L.; Liu, J.; Zhou, O. Adv Mater 2002, 14, 1387–1390.
38. Lopez-Manchado, M. A.; Biagiotti, J.; Valentini, L.; Kenny, J. M. J Appl polym Sci 2004, 92, 3394–3400.
39. Valentini, L.; Biagiotti, J.; Kenny, J. M.; Lopez-Manchado, M. A. J Polym Sci Part B: Polym Phys 2003, 89, 2657–2663.
40. Haggenmueller, R.; Gommans, H. H.; Rinzler, A. G.; Fischer, J. E.; Winey, K. I. Chem Phys Lett 2000, 330, 219–225.
41. Putz, K. W.; Mitchell, C. A.; Krishnamoorti, R.; Green, P. F. J Polym Sci Part B: Polym Phys 2004, 42, 2286–2293.
42. Grady, B. P.; Pompeo, F.; Shambaugh, R. L.; Resasco, D. E. J Phys Chem B 2002, 106, 5852–5858.
43. Du, F.; Fischer, J. E.; Winey, K. I. J Polym Sci Part B: Polym Phys 2003, 41, 3333–3338.
44. Barraza, H. J.; Pompeo, F.; O'Rear, E. A.; Resasco, D. E. Nano Lett 2002, 2, 797–802.
45. Mudarra, M.; Diaz-Calleja, R.; Belana, J.; Canadas, J. C.; Diego, J. A.; Sellares, J.; Sanchis, M. J. Polymer 2001, 42, 1647–1651.
46. Valentini, L.; Puglia, D.; Frulloni, E.; Armentano, I.; Kenny, J. M.; Santucci, S. Compos Sci Technol 2004, 64, 23–33.
47. Bhattacharyya, A. R.; Sreekumar, T. V.; Liu, T.; Kumar, S.; Ericson, L. M.; Hauge, R. H.; Smalley, R. E. Polymer 2003, 44, 2373–2377.
48. Ramanathan, T.; Fisher, F. T.; Ruoff, R. S.; Brinson, L. C. Chem Mater 2005, 17, 1290–1295.
49. Wei, C. Y.; Srivastava, D.; Cho, K. J. Nano Lett 2002, 2, 647–650.
50. Lodge, T. P.; McLeigh, T. C. B. Macromolecules 2000, 33, 5278–5284.
51. Mori, T.; Tanaka, K. Acta Metall 1973, 21, 571–574.
52. Bradshaw, R. D.; Fisher, F. T.; Brinson, L. C. Compos Sci Technol 2003, 63, 1705–1722.
53. Fisher, F. T.; Bradshaw, R. D.; Brinson, L. C. Compos Sci Technol 2003, 63, 1689–1703.
54. Liu, H.; Liao, K. J Appl Polym Sci 2004, 94, 211–221.
55. Franco, R. W. A.; Donoso, J. P.; Magon, C. J.; Rodella, C. B.; Florentino, A. O.; Saeki, M. J.; Pernaut, J. M.; de Oliveria, A. L. Solid State Ionics 1998, 115, 149–160.
56. Carmona, F. Physica A 1989, 157, 461–469.
57. Prasse, T.; Ivankov, A.; Sandler, J.; Schulte, K.; Bauhofer, W. J Appl Polym Sci 2001, 82, 3381–3386.
58. Valentini, L.; Armentano, I.; Puglia, D.; Kenny, J. M. Carbon 2004, 42, 323–329.
59. Chen, R. J.; Bangsaruntip, S.; Drouvalakis, K. A.; Kam, N. W. S.; Shim, M.; Li, Y. M.; Kim, W.; Utz, P. J.; Dai, H. J. Proc Natl Acad Sci USA 2003, 100, 4984–4989.
60. Shim, M.; Javey, A.; Kam, N. W. S.; Dai, H. J. J Am Chem Soc 2001, 123, 11512–11513.